

Article

Preparation of a High-Performance Catalyst Derived from Modified Lignin Carbon for the Hydrogen Evolution Reaction of Electrolyzed Water

Wei Wang ^{1,2} , Liting Qin ^{1,2}, Hongting Tang ^{1,2}, Qinglei Liu ^{1,2,*} and Yongfei Wang ^{3,4,*} 

¹ School of Perfume and Aroma Technology, Shanghai Institute of Technology, 100#, Haiquan Road, Shanghai 201418, China; wangweittg@sit.edu.cn (W.W.); qinliting_3611@163.com (L.Q.); 206071242@mail.sit.edu.cn (H.T.)

² Engineering Research Center of Perfume & Aroma and Cosmetics, Ministry of Education, Shanghai 201418, China

³ School of Chemical Engineering, University of Science and Technology Liaoning, 185#, Qianshan Zhong Road, Anshan 114044, China

⁴ School of Materials and Metallurgy, University of Science and Technology Liaoning, 185#, Qianshan Zhong Road, Anshan 114044, China

* Correspondence: liuqinglei@sit.edu.cn (Q.L.); wyf8307@ustl.edu.cn (Y.W.)

Abstract: Hydrogen energy is a plentiful and environmentally friendly form of secondary energy that could play a crucial role in achieving global energy sustainability. At the same time, the electrolysis of water for hydrogen production is a significant future-oriented advancement in the energy sector, whereas appropriate hydrogen evolution catalysts have always been the key to hydrogen evolution reactions. In this study, lignin was utilized as an appropriate raw material for modification in order to obtain carbon materials, which was then supported with Ru to prepare an Ru_{0.8}@MLC catalyst. At a current density of 10 mA cm⁻², the required overpotential was a mere 35.6 mV and the slope of Tafel was 31.7 mV dec⁻¹. This study provides a feasible strategy and pathway for preparing highly efficient electrocatalysts for the hydrogen evolution reaction.



Citation: Wang, W.; Qin, L.; Tang, H.; Liu, Q.; Wang, Y. Preparation of a High-Performance Catalyst Derived from Modified Lignin Carbon for the Hydrogen Evolution Reaction of Electrolyzed Water. *Catalysts* **2023**, *13*, 1404. <https://doi.org/10.3390/catal13111404>

Academic Editors: Carlo Santoro and Enric Brillas

Received: 21 September 2023

Revised: 23 October 2023

Accepted: 25 October 2023

Published: 29 October 2023



Copyright: © 2023 by the authors. Licensee MDPI, Basel, Switzerland. This article is an open access article distributed under the terms and conditions of the Creative Commons Attribution (CC BY) license (<https://creativecommons.org/licenses/by/4.0/>).

Keywords: ruthenium nanoparticles; lignin; modification; hydrogen evolution reaction

1. Introduction

In our contemporary society, we face the dual challenges of rapid industrialization and a burgeoning population, both of which are contributing to the imminent depletion of fossil energy resources. This scarcity poses a formidable obstacle to the advancement of human civilization. Additionally, the widespread utilization of fossil fuels leads to the emission of harmful gases, primarily CO₂, which not only degrades our living environment but also has a profound impact on our daily lives [1–3]. Through people's exploration and research, hydrogen energy has been found to be a new type of clean and renewable energy that has considerable development prospects; the high energy density of hydrogen energy and the fact that only water is produced after its combustion provide strong support for it replacing fossil energy [4–8]. The electrolysis of water is a viable method for hydrogen production.

However, the electrolysis of water to produce hydrogen still faces huge challenges. In the process of the electrolysis of water, the process of electron transfer is complex; it usually requires a high overpotential (η) and therefore efficient catalysts are usually needed to reduce the overpotential of hydrogen evolution [9–12]. Currently, commercial electrocatalysts are generally Pt-based catalysts; platinum group elements have excellent hydrogen evolution performance, so they are recognized as the best HER catalysts [13–15]. Pt-based catalysts can effectively reduce the overpotential of electrolytic water and accelerate the process of electron transfer. However, Pt-based catalysts are expensive and infrequent in the earth's crust [16–18], which hinders the industrial development and application of

hydrogen evolution via the electrolysis of water [19,20]. Ru is the most cost-effective metal within the platinum group and exhibits hydrogen evolution performance comparable with that of Pt, making it a preferred alternative to Pt [21]. A lot of research on the application of Ru-based electrocatalysts in the field of hydrogen evolution in the electrolysis water is ongoing. Supporting Ru nanoparticles on various anion-doped carbon materials is a commonly adopted approach in the research of Ru-based catalysts. The objective of enhancing the hydrogen evolution reaction (HER) activity of Ru-based catalysts is achieved by modifying the secondary metal active sites and reinforcing the electronic interactions between the active sites and the support material [22]. Currently, significant attention is given to nitrogen (N) doping [23–27], sulfur (S) doping [28–30], phosphorus (P) doping [31–33], or the combined synergistic effects of multiple elements [22,34–36]. Heteroatoms decrease the electronegativity of Ru by transferring the electrons of Ru, thereby enhancing Ru's capability to desorb hydrogen [37,38]. Throughout the hydrogen evolution process, heteroatoms serve a regulatory function rather than acting as active checkpoints, with Ru remaining as the active center for the HER [39]. For instance, Sun et al. employed the “one-pot method” to disperse ultra-small Ru nanoparticles (Ru NPs) on S-doped graphene, resulting in the synthesis of Ru/S-rGO-24. The metal-carrier interaction between S-rGO and Ru NPs facilitated the electron transfer from Ru, leading to the easy breaking of the O-H bond in water, reducing the dissociation energy, and enhancing the electrocatalytic activity [40]. Nitrogen-doped porous carbon substrates were synthesized by Yao et al. using ZIF-8 as the precursor and a SiO_2^- protected calcination strategy. Furthermore, ethylene glycol (EG) was used as a reducing agent and solvent to prepare Ru/PNC using a microwave-assisted method. The experimental results demonstrated that the prepared porous nitrogen-doped carbon (PNC) exhibits high dispersibility, a large specific surface area, and a rich pore structure, enabling significant exposure of active sites [41]. These studies confirm that heteroatom doping plays a crucial role in the formation and effective dispersion of ultra-small Ru (ruthenium) nanoparticles, resulting in the creation of a significantly expanded electrochemically active surface area. This, in turn, exposes a greater number of active sites, contributing to improved catalytic performance. Furthermore, these findings highlight the importance of metal-support interactions in promoting electron deficiency within the Ru nanoparticles, which facilitates the disruption of H-OH bonds, lowers the energy barrier for hydrolysis, and enhances electrocatalytic activity. These insights have profound implications for our research. The outstanding properties of heteroatom-doped carbon substrates in enhancing catalyst performance, coupled with the economical use of ruthenium, indicate that nitrogen-doped ruthenium-containing catalysts hold substantial promise for advancements in the field of hydrogen evolution in electrolytic water. However, it is important to note that Ru nanomaterials with different morphologies exhibit poor stability when they undergo aggregation. Hence, it is crucial to prepare suitable carriers that can effectively support Ru metal particles and enhance their dispersibility. In this research paper, a novel approach was employed where lignin was utilized as a carbon material for the modification and support of ruthenium in the synthesis of hydrogen evolution reaction (HER) catalysts.

Lignin is a biomass raw material with a high yield [42]. It boasts a complex three-dimensional network structure and stands as the only naturally occurring product with an aromatic structure among natural polymers [43,44]. However, lignin molecules lack strong hydrophilic functional groups and exhibit an insufficiency of active sites for reactions. Additionally, they display certain shortcomings in terms of hydrophilicity and chemical reactivity. These limitations restrict the scope of lignin's applications. As such, the activation or modification of lignin becomes a pivotal research approach aimed at enhancing its practical utility. At present, the methods of activation and modification of lignin are usually sulfonation, graft modification, cross-linking reactions and oxidative ammonolysis [45]. Lignin is regarded as an ideal source for the production of carbon materials due to its abundant availability and distinctive physical and chemical properties. Furthermore, the resulting carbon materials have found extensive applications in both industrial and

everyday life. These applications include organic waste gas adsorption [46], electrode materials [47], super capacitors [48,49] and more.

In this paper, a well-distributed ruthenium-containing nano-catalyst was prepared using modified lignin as a carbon precursor material; the Ru was anchored on the lignin after ammonolysis. Firstly, the lignin was modified by ammonia, which not only increased the reaction activity of lignin but also increased the content of total nitrogen and available nitrogen in lignin, and then mixed with RuCl_3 for the hydrothermal loading of Ru, and finally it was calcined and reduced with Ru^{3+} at a high temperature to prepare Ru-containing catalysts with moderate sizes and uniform dispersions, i.e., $\text{Ru}_x\text{@MLC}$ (Ru-containing modified lignin carbon) catalysts. In an alkaline environment, the catalysts exhibited a superior HER catalytic performance compared with the commercial 20 wt% Pt/C. This study provides a feasible preparation strategy for the rational synthesis of cost-effective Ru-based catalysts with excellent performance and broad applicability.

2. Results and Discussion

In this work, we used lignin as a catalyst carrier and RuCl_3 as a Ru source to synthesize $\text{Ru}_x\text{@MLC}$ catalysts for hydrogen evolution from electrolytic water via hydrothermal synthesis. The preparation process of the $\text{Ru}_{0.8}\text{@MLC}$ catalyst is shown in Figure 1.

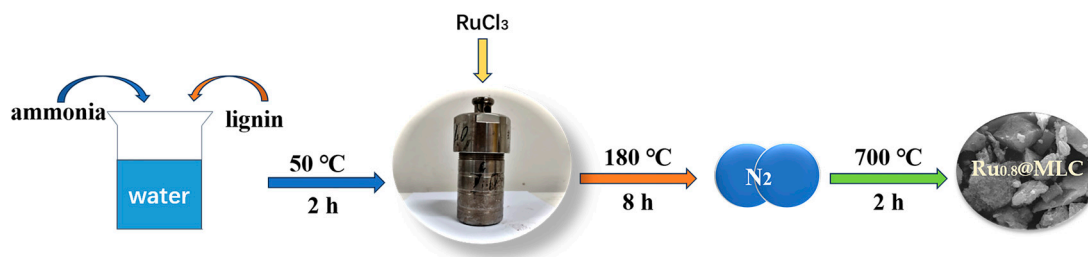


Figure 1. Synthesis process of $\text{Ru}_{0.8}\text{@MLC}$.

First of all, the morphology of the prepared $\text{Ru}_{0.8}\text{@MLC}$ catalyst was observed by scanning electron microscopy (SEM). As shown in Figure 2a,b, the loose blocky structure of the $\text{Ru}_{0.8}\text{@MLC}$ catalyst can be obviously observed. It is also obvious from the diagram that the prepared catalyst is uniformly dispersed and there are no adverse conditions such as agglomeration and hardening. In order to observe the microscopic morphology of the catalyst in more detail, images obtained through transmission electron microscopy (TEM) are shown in Figure 2c,d. It is clear that Ru nanoparticles are uniformly supported on the carbon materials.

Figure 2e is a histogram illustrating the particle size distribution of the Ru nanoparticles in Figure 2d. This histogram reveals that the average particle size of the Ru nanoparticles is approximately 3 nm. Finally, Figure 2f is a high-resolution TEM (HRTEM) image where easily recognizable Ru lattice fringes are visible and have approximate spacings of 0.205 nm and 0.234 nm, which correspond to Ru's 101 and 100 crystal planes, respectively. Figure 3 is the $\text{Ru}_{0.8}\text{@MLC}$ catalyst's EDS element map image, which shows the distribution of the C, N, O and Ru elements. This observation confirms the successful incorporation of nitrogen (N) into the carbon materials. Simultaneously, it provides further evidence of the effective loading of the ruthenium (Ru) element onto the carbon materials.

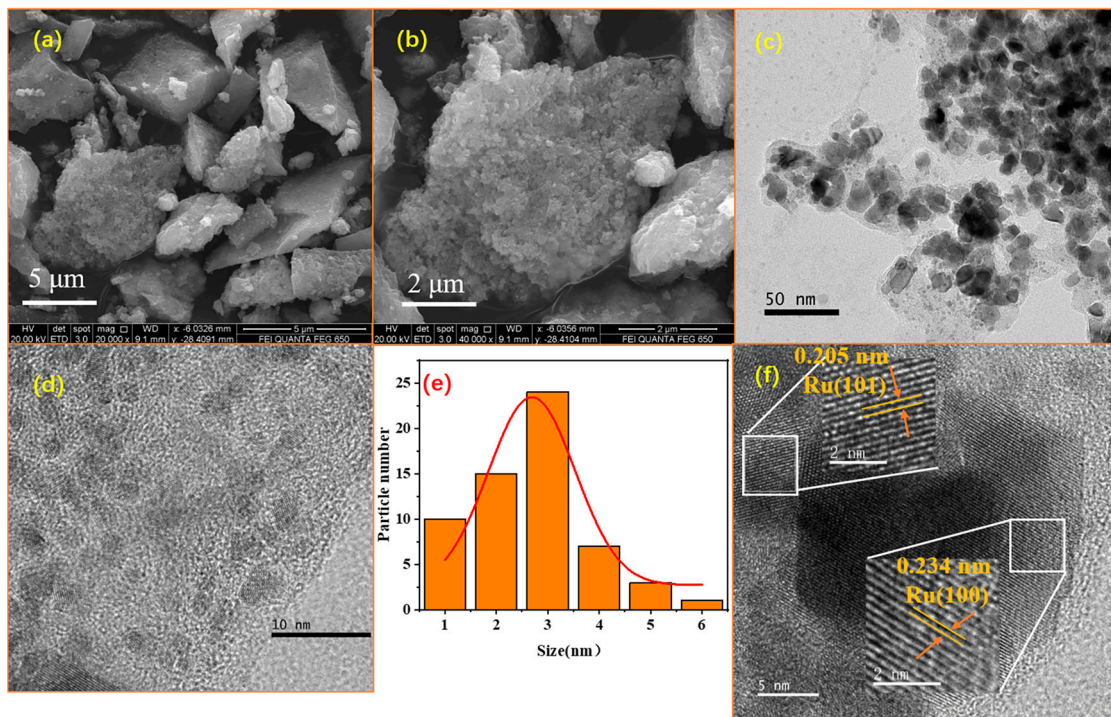


Figure 2. SEM images of Ru_{0.8}@MLC (a,b); TEM images of Ru_{0.8}@MLC (c,d); size distribution in Ru_{0.8}@MLC (e); HRTEM image of Ru_{0.8}@MLC (f).

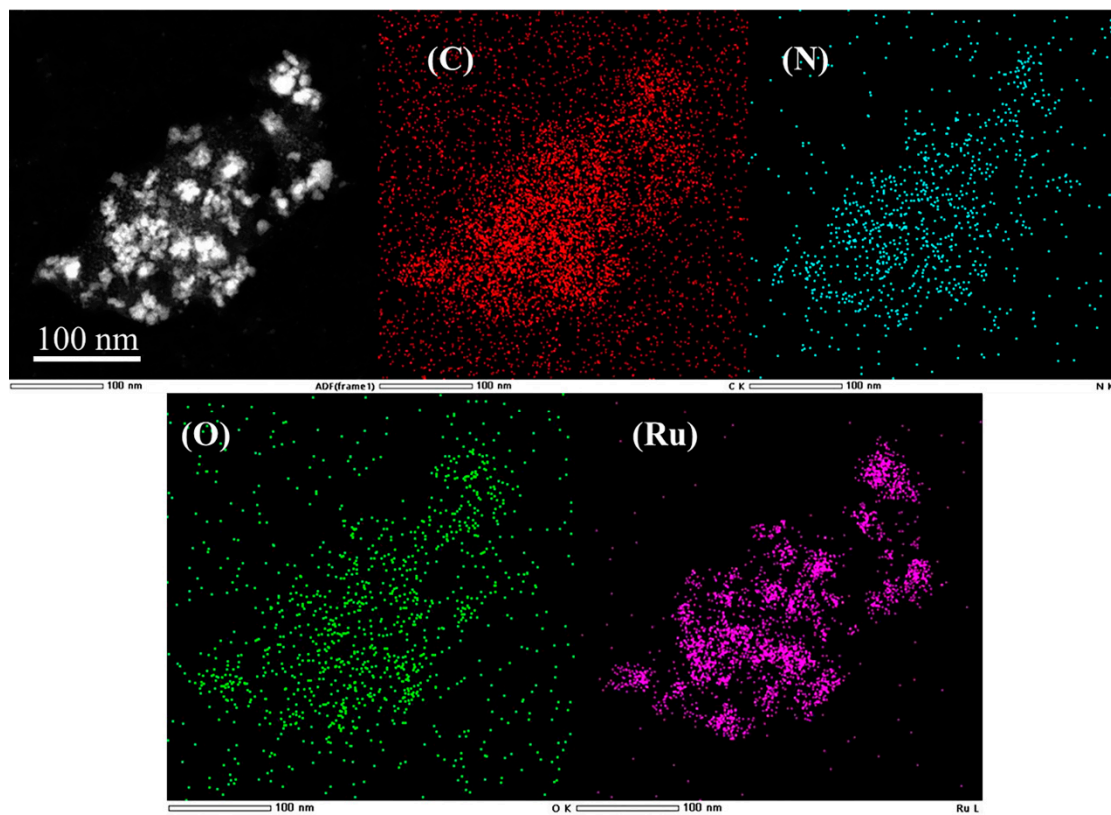


Figure 3. STEM-EDS image of Ru_{0.8}@MLC and its corresponding elemental mapping of C, N, O and Ru.

Subsequently, the crystal structure of the $\text{Ru}_x\text{@MLC}$ catalysts was examined and characterized using X-ray diffraction (XRD). As depicted in Figure 4, the diffraction peaks at 2θ angles of 38.3° , 42.2° , 44.0° , 58.4° , 69.4° and 78.3° are notably prominent for the five catalysts. These peaks correspond to the crystal planes of Ru [4], indicating that the Ru molecules in the aforementioned catalysts are effectively supported on the modified lignin. As anticipated in this study, an increase in the quantity of RuCl_3 added to the reaction results in higher peak intensities, particularly on the crystal planes of (100) and (101). As the quantity of RuCl_3 increases, there is a noticeable enhancement in the peak intensity. This observation indicates that when RuCl_3 serves as the source of ruthenium, a higher Ru content facilitates the formation of ruthenium crystals during the preparation process. Therefore, the precise control of the metal content plays a pivotal role in the electrocatalyst synthesis. Likewise, the XRD patterns of all the catalyst samples exhibit diffraction peaks corresponding to the 002 crystal plane of graphitized carbon at a diffraction angle of 26.4° . The presence of this diffraction peak shows that the carbon materials produced possess a certain degree of graphitization tendency, indicating their substantial electrical conductivity.

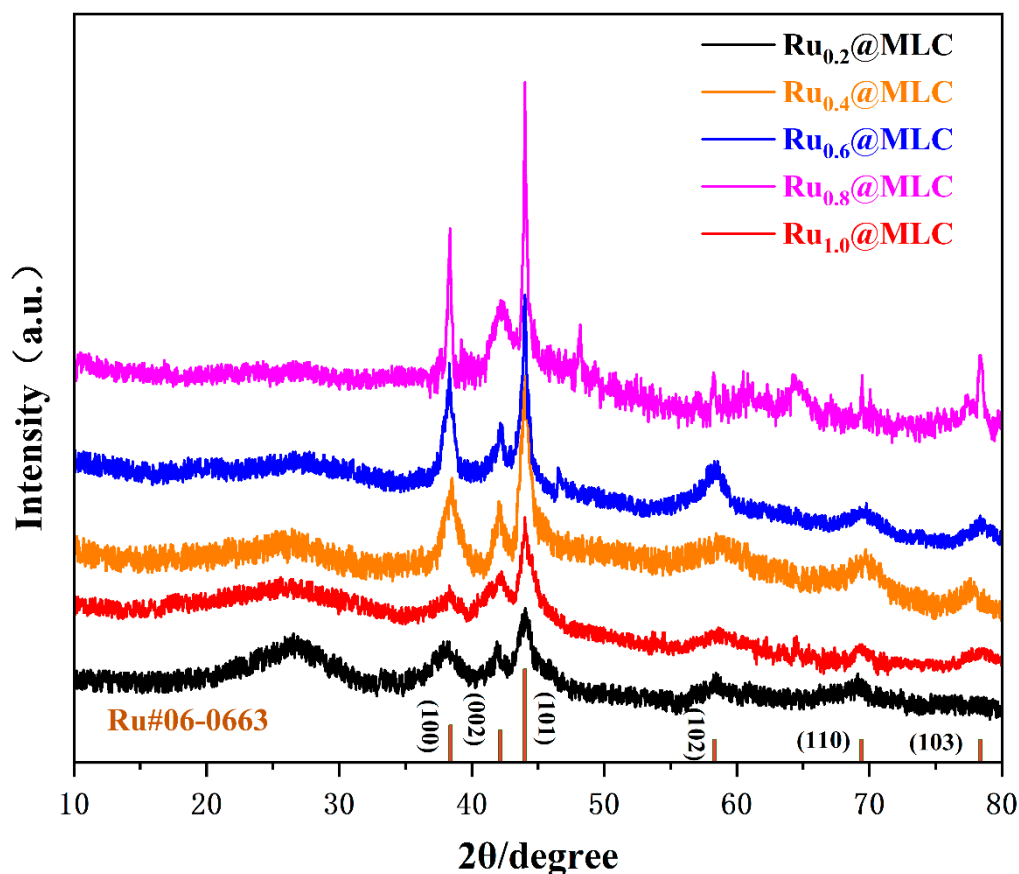


Figure 4. XRD spectra of $\text{Ru}_{0.2}\text{@MLC}$, $\text{Ru}_{0.4}\text{@MLC}$, $\text{Ru}_{0.6}\text{@MLC}$, $\text{Ru}_{0.8}\text{@MLC}$ and $\text{Ru}_{1.0}\text{@MLC}$.

The Raman spectra of the $\text{Ru}_x\text{@MLC}$ catalysts can be found in Figure S1 of the Supporting Information (SI). The analysis of Figure S1 shows that the sample appears as two strong peak signals near 1350 cm^{-1} and 1591 cm^{-1} that correspond to disordered carbon (D band) and ordered graphitic carbon (G band) [50,51], respectively. Similar to the previously reported doped graphite materials, the degree of defects inside the crystal structure of the catalyst can be judged by comparing the ratio of the strength (ID) of the material at the D peak to the strength (IG) at the G peak [52,53]. The greater the intensity of the D peak, the more disordered the carbon with lattice defects represented by the D peak in the prepared catalyst; the lattice defects contribute to electron transfer. The more defects inside the material, the stronger the crystal's conductivity [54]. In addition, the reported G

band of N-doped graphene is generally narrower than the D band [55–57]. In our study, the G band is wider than the D band (Figure S1), which further indicates that there are more defect checkpoints in the prepared nitrogen-doped carbon nanomaterials. As depicted in Figure S1, the ID/IG ratio of each catalyst steadily increases when the concentration of the Ru solution used in the preparation is increased; the initial ratio is approximately 0.801. This phenomenon primarily stems from the disruption of the structural crystal within the carbon material upon the introduction of Ru elements. This observation indicates that the carbon nanomaterials synthesized using this approach exhibit good electrical conductivity. However, the incorporation of Ru elements leads to an increase in the internal defects and an accelerated electron transfer rate, ultimately conferring several advantages for enhancing the electrocatalytic activity of these catalytic materials.

X-ray photoelectron spectroscopy (XPS) was used to characterize the chemical state and electronic configuration of the Ru_{0.8}@MLC catalyst's surface. The findings were charge corrected using the benchmark of the standard characteristic peak at 284.6 eV in the C1s orbital and are depicted in Figure 5. Figure 5a illustrates the full XPS spectrum, which clearly shows the presence of both carbon (C) and nitrogen (N) in Ru_{0.8}@MLC. The presence of these elements indicates the successful integration of ruthenium into the catalyst.

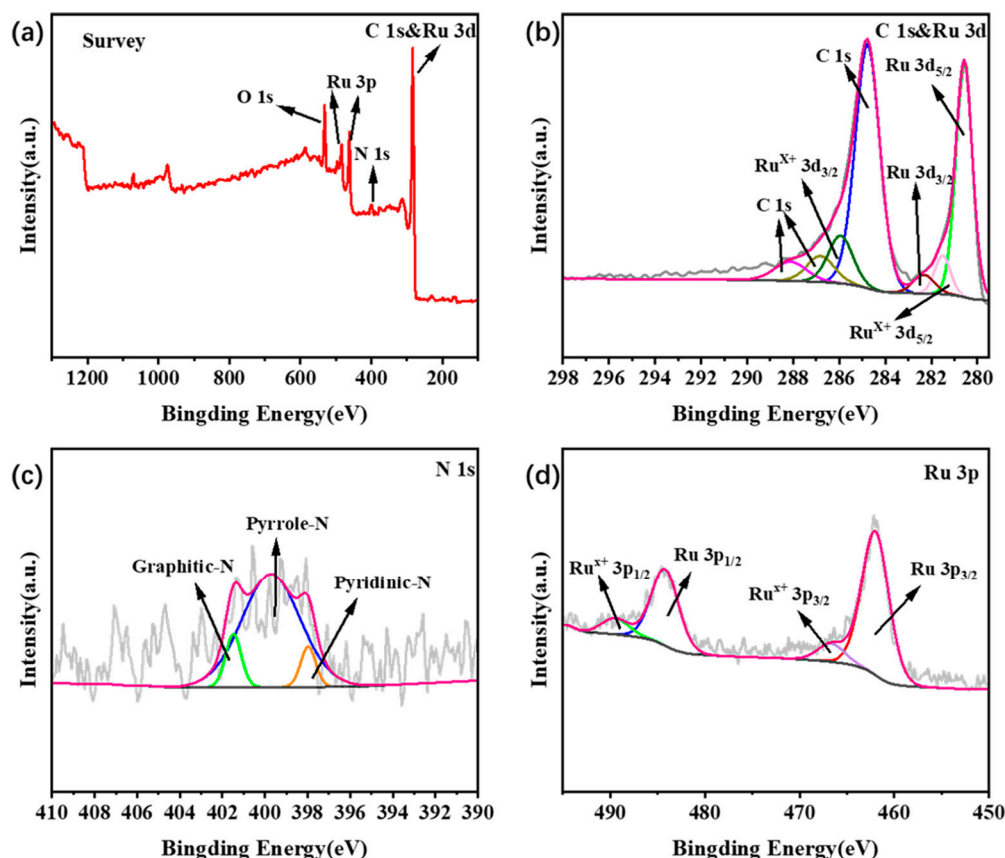


Figure 5. Full XPS spectrum of Ru_{0.8}@MLC (a) and the high-resolution spectra of the C 1s and Ru 3d, N 1s and Ru 3p of Ru_{0.8}@MLC (b–d).

The XPS findings for C 1s and Ru 3d are presented in Figure 5b. As shown in the figure, the fitted peaks corresponding to C-O and C=O are observed at binding energies of 286.4 eV and 288.5 eV, respectively. The peaks centered at 282.7 eV and 286.1 eV correspond to Ru 3d_{3/2} and Ru^{x+} 3d_{3/2}, whereas the peaks at 280.6 eV and 281.8 eV correspond to Ru 3d_{5/2} and Ru^{x+} 3d_{5/2}, respectively [58–61]. As demonstrated in Figure 5c, distinct fitting peaks are observed for graphite nitrogen, pyrrole nitrogen and pyridine nitrogen at 401.5 eV, 399.7 eV and 397.9 eV, respectively. This is basically consistent with the peak positions reported by existing studies [60]. The inclusion of graphitized nitrogen significantly enhances the

conductivity of carbon groups, whereas pyrrole nitrogen and pyridine nitrogen effectively adsorb specific cations [62–65].

Finally, in Figure 5d, we present the high-resolution XPS fitting of Ru 3p. Notably, the peaks at 461.6 eV and 465.6 eV correspond to the characteristic peaks of Ru 3p_{3/2} and Ru^{x+} 3p_{3/2}, respectively. In addition, the peaks at 484.5 eV and 488.1 eV correspond to the characteristic peaks of Ru 3p_{1/2} and Ru^{x+} 3p_{1/2}, respectively. It is worth mentioning that the presence of Ru^{x+} indicates the oxidation of some ruthenium particles on the sample surface. Upon comparing the peak areas, it becomes evident that, despite the coexistence of Ru and Ru^{x+}, the content of Ru surpasses that of Ru^{x+}. This observation suggests a significant reduction in the Ru³⁺ originating from RuCl₃.

The electrochemical performance tests for the hydrogen evolution reaction (HER) were carried out using a three-electrode system with a 1 M KOH electrolyte (alkaline, pH = 14) under a nitrogen atmosphere at room temperature. In Figure 6a, the polarization curve in the 1 M KOH electrolyte solution is presented. It is noteworthy that all catalysts exhibit an initial potential very close to zero. As the voltage increases, once the current density reaches 10 mA cm⁻², the overpotentials for Ru_{0.2}@MLC, Ru_{0.4}@MLC, Ru_{0.6}@MLC, Ru_{0.8}@MLC, Ru_{1.0}@MLC and the 20 wt% commercial Pt/C catalyst are determined to be 270.6 mV, 129.2 mV, 75.5 mV, 35.6 mV, 41.7 mV and 37.2 mV, respectively.

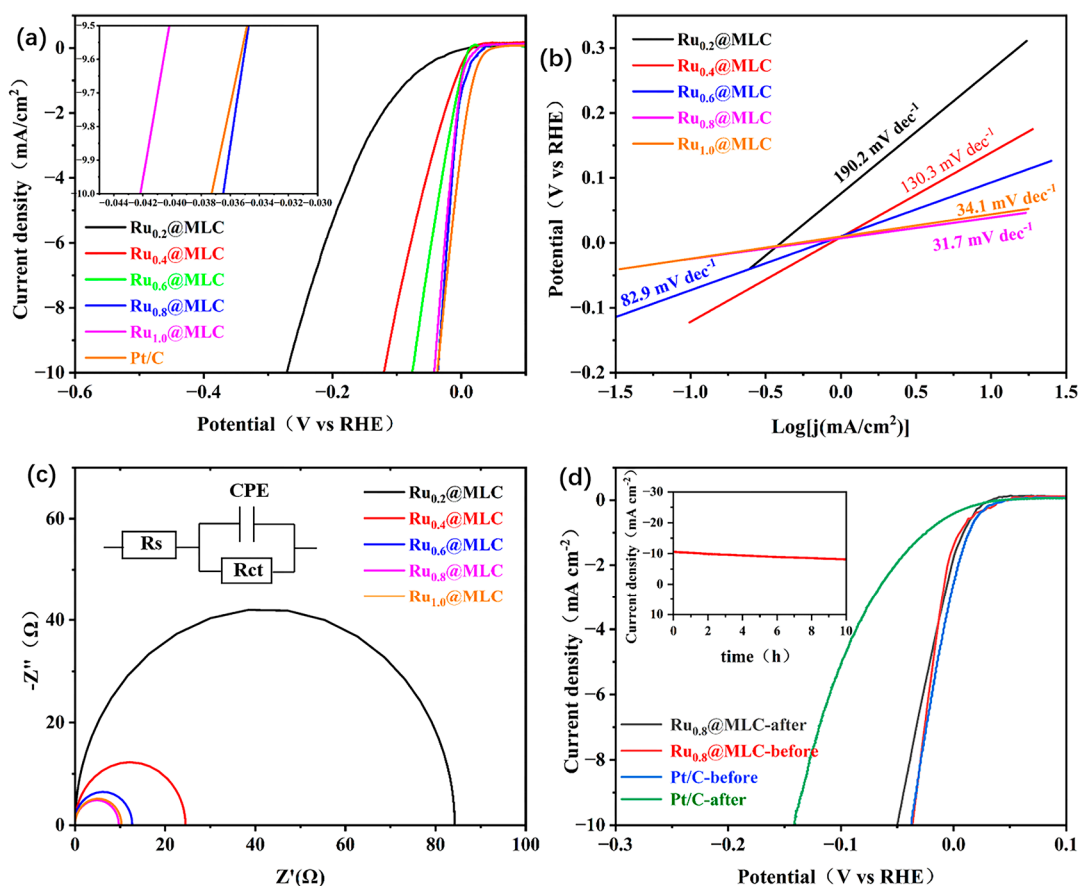


Figure 6. HER polarization curves of Ru_{0.2}@MLC, Ru_{0.4}@MLC, Ru_{0.6}@MLC, Ru_{0.8}@MLC, Ru_{1.0}@MLC and 20%wt Pt/C (a); Tafel slope diagram (b); Nyquist curves (c); durability test for Ru_{0.8}@MLC and 20%Pt/C before and after 2000 cycles of cyclic voltammetry in 1 M KOH (d).

It is not difficult to find that the activity of the catalyst enhances gradually with the increase in Ru loading. The catalyst exhibits its optimal catalytic performance when the amount of added RuCl₃ is 0.8 g, as evidenced by the results obtained for Ru_{0.8}@MLC. However, when the quantity of RuCl₃ used is increased to 1.0 g, the catalyst's performance is inferior to that of the 0.8 g quantity. This observation indicates that the electrocatalytic

hydrogen evolution performance of the catalyst cannot be indefinitely improved by simply increasing the amount of RuCl_3 used. The catalyst's catalytic performance exhibits a trend of initially increasing and then decreasing with the Ru content. This phenomenon may be attributed to an excessive amount of Ru being added surpassing the carbon material's uniform loading capacity. The surplus Ru element cannot be uniformly dispersed on the carbon material, leading to agglomeration, which subsequently impacts the catalyst's catalytic performance.

Further, the reaction mechanism of the samples at different Ru contents was explored by Tafel analysis. Figure 6b shows the Tafel slopes of several $\text{Ru}_x\text{@MLC}$ ($\text{Ru}_{0.2}\text{@MLC}$, $\text{Ru}_{0.4}\text{@MLC}$, $\text{Ru}_{0.6}\text{@MLC}$, $\text{Ru}_{0.8}\text{@MLC}$ and $\text{Ru}_{1.0}\text{@MLC}$) catalysts under alkaline conditions. The corresponding Tafel slopes were found to be $190.2 \text{ mV dec}^{-1}$, $130.3 \text{ mV dec}^{-1}$, 82.9 mV dec^{-1} , 31.7 mV dec^{-1} and 34.1 mV dec^{-1} for the respective catalysts. The results indicate that under alkaline conditions, the rate-determining step for $\text{Ru}_{0.2}\text{@MLC}$ and $\text{Ru}_{0.4}\text{@MLC}$ is the Volmer reaction (hydrogen adsorption), whereas the Herovskyy reaction involving electrochemical desorption is the rate-determining step for the HER reaction process of the other catalysts. We speculate that with the increase in Ru content, the contents of Ru and Ru^{x+} in the catalyst also increase accordingly. The increase in Ru content is beneficial to the formation of Ru nanoclusters, thereby enhancing the strong electronic coupling effect between Ru nanoclusters and single-atom Ru^{x+} in the catalyst, which is beneficial to realize the rapid dissociation of water and optimize the H^* strength of metal adsorption [66], which, in turn, promotes the Volmer reaction and results in the change in the RDS mechanism from low Ru content to high Ru content. Surprisingly, we also found a similar pattern in Zhang et al.'s research report [67]. This study revealed that the introduction of Ru atoms into NiFe-LDH can efficiently reduce the energy barrier of the Volmer step, eventually accelerating its HER kinetics. Moreover, this shows that with an increase in the Ru atom content, the prepared NiFeRu-LDH nanosheets have a smaller size and greater roughness, and beyond a certain Ru content, agglomeration of nanoparticles is observed. The Tafel plot of NiFeRu-LDH was as low as 31 mV dec^{-1} , which was much lower than the 132 mV dec^{-1} for the Ni foam, 153 mV dec^{-1} for NiFe-LDH and 32 mV dec^{-1} for the Pt/C catalyst. In addition, the HER polarization curve of NiFeRu-LDH is negatively shifted with an increase in Ru content.

In Figure 6c, an equivalent circuit model is presented for impedance fitting, illustrating the electrochemical impedance spectra of the $\text{Ru}_{0.2}\text{@MLC}$, $\text{Ru}_{0.4}\text{@MLC}$, $\text{Ru}_{0.6}\text{@MLC}$, $\text{Ru}_{0.8}\text{@MLC}$ and $\text{Ru}_{1.0}\text{@MLC}$ samples under alkaline conditions. Within this model, R_{ct} represents the charge transfer resistance, R_s signifies the solution resistance and C_{pe} denotes the equivalent capacitive element. Notably, the $\text{Ru}_{0.8}\text{@MLC}$ catalyst, prepared with 0.8 g of RuCl_3 , exhibits the lowest charge resistance, the highest charge transfer rate and displays impedance curves with the smallest semicircle radius. The impedance semicircles for the other catalysts aligns closely with the performances observed in the polarization curves. These results indicate that $\text{Ru}_{0.8}\text{@MLC}$ displays faster interfacial charge transfer kinetics in the hydrogen evolution reaction (HER) process, reflecting its electrochemical catalytic hydrogen evolution performance. Stability is another important index for evaluating the performance of electrocatalysts. The curves shown in Figure 6d are the polarization curves of $\text{Ru}_{0.8}\text{@MLC}$ and Pt/C before and after 2000 cycle voltamperes. It is obvious that after 2000 cycles of CV, the catalytic performance of Pt/C decreases and the stability of $\text{Ru}_{0.8}\text{@MLC}$ is greater than that of Pt/C. After 2000 cycles of CV, the overpotential of $\text{Ru}_{0.8}\text{@MLC}$ is reduced by only 14 mV at a current density of 10 mA cm^{-2} , ranging from 35.6 mV to 49.6 mV. Figure 6d illustrates the constant voltage curve for $\text{Ru}_{0.8}\text{@MLC}$ at an overpotential of 10 mA cm^{-2} . This curve demonstrates that even after 10 h of testing, the current density remains above 80.3% of the initial value, decreasing from 10 mA cm^{-2} to 8.03 mA cm^{-2} , underscoring the catalyst's high stability. The catalytic stability of $\text{Ru}_{0.8}\text{@MLC}$ is excellent compared with the previously reported Ru-based carbon-supported catalytic systems; it has a lower Tafel slope (31.7 dec^{-1}) and a lower overpotential (35.6 mV)

than Ru@CQDs800 [68], Ru@CN-0.16 [69], Ru S/DA [70] and Ru/C (5 wt 25%) [71], as presented in Table 1.

Table 1. Comparison the electrochemical activity of Ru_{0.8}@MLC with other previously reported Ru-based carbon-supported catalytic systems.

Catalyst Name	Tafel Slope (dec ⁻¹)	V _{10 mA·cm⁻²} (mV)	Stability (V _{10 mA·cm⁻²} , 1 M KOH)
Ru _{0.8} @MLC	31.7	35.6	49.6 mV (After 2000 cycles of CV)
Ru@CQDs800	63	65	69 mV (After 2000 cycles of CV)
Ru@CN-0.16	53	32	a slight increase in overpotential after 2000 cycles
Ru S/DA	90	58	73 mV (After 5000 cycles of CV)
5 wt% Ru/C	73	55	126 mV (After 10,000 cycles of CV)

To investigate the electrochemical active surface area (ECSA) and catalytic activity of the samples, cyclic voltammetry curves were measured for Ru_{0.2}@MLC, Ru_{0.4}@MLC, Ru_{0.6}@MLC, Ru_{0.8}@MLC and Ru_{1.0}@MLC at various scanning rates. The double-layer capacitance (C_{dl}) of the samples was determined. The scanning rate for the cyclic voltammetry curve commenced at 20 mV s⁻¹ and was subsequently increased by 20 mV s⁻¹ until reaching 100 mV s⁻¹. The results are illustrated in Figure 7. The C_{dl} values for different catalysts were obtained and used to derive the ECSA and other relevant information, as presented in Table 2. These findings unequivocally indicate that Ru_{0.8}@MLC possesses a higher number of active surface sites.

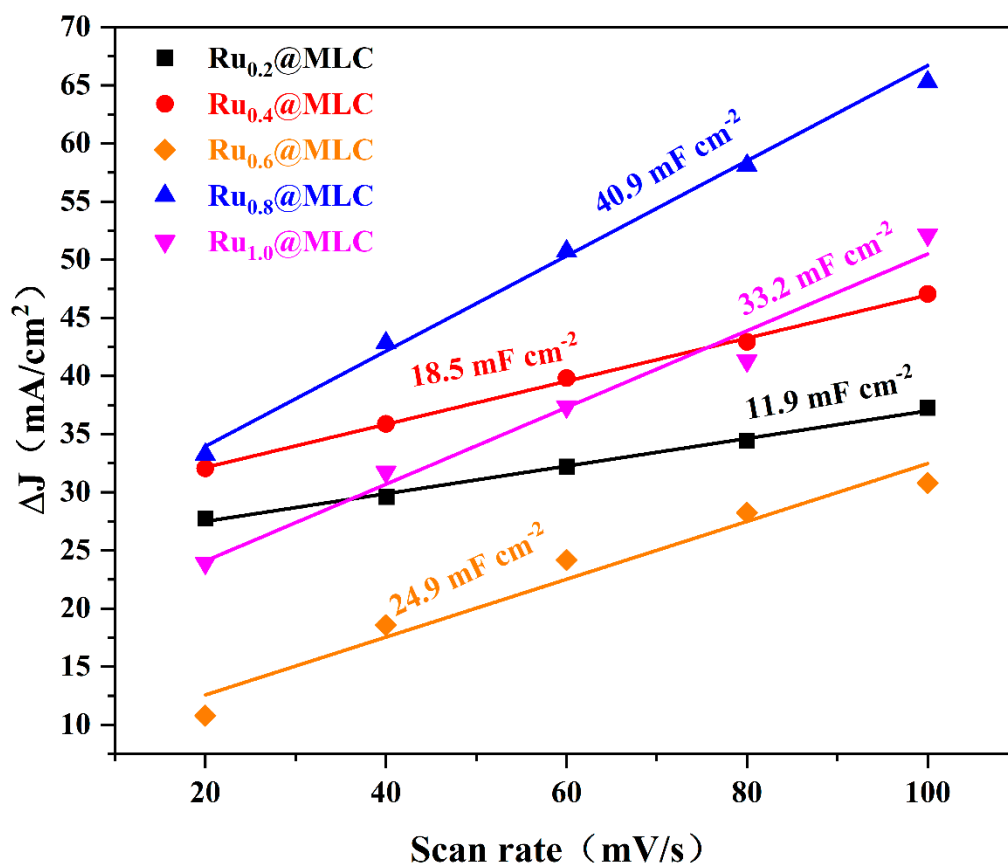


Figure 7. Function of current density and scanning rate of Ru_{0.2}@MLC, Ru_{0.4}@MLC, Ru_{0.6}@MLC, Ru_{0.8}@MLC and Ru_{1.0}@MLC.

Table 2. Comparison of the electrochemical active surface area (ECSA) and catalytic activity of several catalysts.

Samples	C_{dl} (mF/cm ²)	C_{DL} (mF)	ECSA (cm ²)
Ru _{0.2} @MLC	11.9	0.833	41.65
Ru _{0.4} @MLC	18.5	1.295	64.75
Ru _{0.6} @MLC	24.9	1.743	87.15
Ru _{0.8} @MLC	40.9	2.863	143.15
Ru _{1.0} @MLC	33.2	2.324	116.2

$$C_{DL} = C_{dl} \times 0.07 \text{ cm}^2; \text{ECSA} = C_{DL}/C_s; C_s = 0.02 \text{ mF cm}^{-2}.$$

C_{DL} and C_s represent the double layer capacitance and specific capacitance, respectively [72,73]. The C_s in alkaline solution was 0.020 mF cm^{-2} ; C_{dl} is the slope obtained by plotting the difference between the absolute value of the current density at different scanning rates and the corresponding scanning rates [74]. The effective area of the catalyst supported on the electrode during the test is 0.07 cm^2 .

3. Experimental Section

3.1. Materials and Methods

In this work, we used lignin as a catalyst carrier and RuCl_3 as a Ru source to synthesize $\text{Ru}_x\text{@MLC}$ catalysts for hydrogen evolution from electrolytic water by hydrothermal synthesis. The process was as follows: Weigh out 25 g of alkaline lignin and dissolve it in 250 mL of deionized water. Stir the mixture slowly until the lignin is completely dissolved, then filter out any insoluble impurities to obtain a lignin solution. Take 25 mL of the prepared lignin solution and heat it to $50 \text{ }^\circ\text{C}$ in an oil bath. While stirring continuously, slowly add 2.5 mL of ammonia water to the solution. Reflux the mixture at a constant temperature of $50 \text{ }^\circ\text{C}$ for 2 h to obtain the modified lignin solution. Remove most of the water from the solution by rotary evaporation, then dry it at $50 \text{ }^\circ\text{C}$ in an oven. Weigh 1.2 g of the modified lignin, disperse it in 20 mL of deionized water (the standard amount of modified lignin used in this study was 1.2 g) and stir slowly until the lignin is completely dissolved. Weigh out 0.2 g, 0.4 g, 0.6 g, 0.8 g or 1.0 g of RuCl_3 and dissolve in the above solution. Then, sonicate the solution in an ice water bath for 0.5 h to evenly disperse the solute. After reacting in a hydrothermal reactor at $180 \text{ }^\circ\text{C}$ for 8 h, filter and dry to obtain a solid containing Ru. The obtained Ru-containing solid was calcined at $700 \text{ }^\circ\text{C}$ under N_2 protection for 2 h to obtain black solid powder as a Ru-containing catalyst, i.e., $\text{Ru}_x\text{@MLC}$ ($X = 0.2, 0.4, 0.6, 0.8$ and 1.0).

3.2. Physicochemical Characterization

In this study, we employed various analytical techniques to characterize the catalyst $\text{Ru}_{0.8}\text{@MLC}$:

Scanning Electron Microscopy (SEM): The morphology of the $\text{Ru}_{0.8}\text{@MLC}$ catalyst was observed using an scanning electron microscope (FEI Quanta FEG 650, FEI, MA, USA). Pure platinum was utilized as a reference material for SEM testing.

Transmission Electron Microscopy (TEM): For precise microscopic examination, we used TEM. The catalyst sample was dispersed in an ethanol solution and sonicated. Subsequently, a few drops of the dispersed liquid were carefully placed on a copper mesh. After the solution dried, we captured high-resolution TEM images (JEOL JEM-F200, accelerating voltage: 200 kV, JEOL, TKY, Japan) and conducted an energy spectrum surface scan (JED-2300T, JEOL, TKY, Japan). This analysis revealed clear Ru lattice fringes. We also mapped the distribution of the C, N, O and Ru elements through EDS element mapping.

X-ray Diffraction (XRD): The crystal structures of the $\text{Ru}_x\text{@MLC}$ catalysts were examined using XRD. We employed a Ritsuya Corporation D/max 2200 PC type X-ray powder diffractometer (JEOL, TKY, Japan) in a scanning range of 10 to 80° at a 2θ angle, with $\text{Cu-K}\alpha$ as the target material.

Raman Spectroscopy: We assessed the degree of graphitization of the samples using a Thermo Fisher DXR (Thermo Fisher, MA, USA) laser Raman spectrometer.

X-ray Photoelectron Spectroscopy (XPS): To analyze the surface chemical state and electronic configuration of the Ru_{0.8}@MLC catalyst, we conducted XPS analysis with a ThermoFisher instrument (model ESCALAB 250 Xi, MA, USA). The analysis chamber was maintained at a vacuum pressure of 8×10^{-10} Pa and we used Al K α rays with a photon energy of 1486.8 eV as the excitation source. The XPS parameters included a working voltage of 12.5 kV, a filament current of 16 mA, and signal accumulation for 10 cycles. During the analysis, we applied a passing energy of 40 eV and a step size of 0.1 eV, with charge correction based on the binding energy of C 1s at 284.60 eV as the energy standard.

3.3. Electrochemical Performance Testing

Electrocatalytic testing of the prepared catalysts was conducted at room temperature using a standard three-electrode system. A glassy carbon electrode (GCE) with a diameter of 3 mm served as the working electrode, whereas a platinum electrode and an Ag/AgCl electrode (3.5 M KCl) functioned as the counter electrode and reference electrode, respectively. The experimental electrolyte solution consisted of 1 M KOH (alkaline, pH = 14), and a continuous stream of N₂ was introduced during all electrochemical tests. Before each test, the catalyst underwent activation through a cyclic voltammetry curve (CV). For electrochemical impedance spectroscopy (EIS): First test the open-circuit voltage. After the open-circuit voltage is stable, then select the determined overpotential for testing. The intersection coordinate value of the low frequency region and the horizontal axis in the impedance spectrum is the charge transfer resistance value (R_{ct}), and the intersection coordinate value of the high frequency region and the horizontal axis in the impedance spectrum is the solution internal resistance (R_s).

4. Conclusions

In the work, we used alkaline lignin as the original material, obtained modified lignin through ammonolysis modification and increased the content of total nitrogen and available nitrogen in the lignin. Then, using a hydrothermal synthesis method and RuCl₃ as the metal Ru source, we loaded the Ru onto the modified lignin. Finally, we calcined and reduced Ru at high temperature to obtain the electrolysis hydrogen evolution catalyst Ru_{0.8}@MLC, which had good catalytic performance and good stability. The three-electrode system showed the good catalytic activity of Ru_{0.8}@MLC in 1 M KOH medium. At a current density of 10 mA cm⁻², the required overpotential was a mere 35.6 mV and the slope of Tafel was 31.7 mV dec⁻¹; Ru_{0.8}@MLC also showed high stability. In this paper, different preparation conditions were also explored, including different activation methods and different Ru reduction temperatures to prepare the catalysts (for more information see the SI). We compared the performance differences of the different catalysts in order to determine the optimal preparation conditions: first, after the ammonolysis of lignin, then using 0.8 g RuCl₃ as metal Ru source, loading by hydrothermal synthesis, and finally calcining at 700 °C to reduce Ru. The Ru_{0.8}@MLC catalysts prepared using this step-by-step method had the best catalytic performance. This study provides a feasible strategy and pathway for preparing highly efficient electrocatalysts for the HER in alkaline environments.

Supplementary Materials: The following supporting information can be downloaded at: <https://www.mdpi.com/article/10.3390/catal13111404/s1>, Figure S1: Raman Spectrum of Ru_{0.2}@MLC, Ru_{0.4}@MLC, Ru_{0.6}@MLC, Ru_{0.8}@MLC and Ru_{1.0}@MLC.

Author Contributions: Conceptualization, W.W. and Q.L.; methodology, L.Q. and H.T.; software, L.Q. and H.T.; validation, L.Q. and H.T.; formal analysis, H.T.; investigation, L.Q., H.T. and Q.L.; resources, W.W. and Q.L.; data curation, L.Q. and H.T.; writing—original draft preparation, L.Q. and H.T.; writing—review and editing, W.W., Q.L. and Y.W.; visualization, L.Q. and H.T.; supervision, W.W. and Q.L.; project administration, W.W. and Q.L.; funding acquisition, W.W. All authors have read and agreed to the published version of the manuscript.

Funding: This research received no external funding.

Data Availability Statement: Not applicable.

Conflicts of Interest: The authors declare that they have no known competing financial interest or personal relationships that could have appeared to influence the work reported in this paper.

References

1. Liang, Y.; Liu, Q.; Asiri, A.M.; Sun, X.; Luo, Y. Self-Supported FeP Nanorod Arrays: A Cost-Effective 3D Hydrogen Evolution Cathode with High Catalytic Activity. *ACS Catal.* **2014**, *4*, 4065–4069. [[CrossRef](#)]
2. Alam, Z.; Verma, B.; Sinha, A.S.K. Effect of preparation on opto-electrical properties of CdS /N, S-rGO photocatalyst for splitting of water by visible light. *Mater. Chem. Phys.* **2020**, *249*, 123212. [[CrossRef](#)]
3. Züttel, A.; Remhof, A.; Borgschulte, A.; Friedrichs, O.; Sciences, E. Hydrogen: The future energy carrier. *Philos. Trans. R. Soc. A Math. Phys. Eng. Sci.* **2010**, *368*, 3329–3342. [[CrossRef](#)] [[PubMed](#)]
4. Tee, S.Y.; Lee, C.J.J.; Dinachali, S.S.; Lai, S.C.; Williams, E.L.; Luo, H.-K.; Chi, D.; Andy Hor, T.S.; Han, M.-Y. Amorphous ruthenium nanoparticles for enhanced electrochemical water splitting. *Nanotechnology* **2015**, *26*, 415401. [[CrossRef](#)] [[PubMed](#)]
5. Patel, R.; Park, J.T.; Patel, M.; Dash, J.K.; Gowd, E.B.; Karpoomath, R.; Mishra, A.; Kwak, J.; Kim, J.H. Transition-metal-based layered double hydroxides tailored for energy conversion and storage. *J. Mater. Chem. A* **2018**, *6*, 12–29. [[CrossRef](#)]
6. Gray, H.B. Powering the planet with solar fuel. *Nat. Chem.* **2009**, *1*, 7. [[CrossRef](#)]
7. Vazhayil, A.; Thomas, J.; Kumar, P.P.A.; Thomas, N. Hydrogen Production from Water Electrolysis: The Role of OER and HER Electrocatalysts. *ACS Symp. Ser.* **2023**, *1435*, 73–119. [[CrossRef](#)]
8. Kumar, M.; Singh, N.K.; Prajapati, K.B.; Kumar, R.S.; Singh, R. Recent Advancements in Nano-Metal-Based Electrocatalysts: Green Hydrogen Production and Storage. *ACS Symp. Ser.* **2023**, *1435*, 43–71. [[CrossRef](#)]
9. Shah, K.; Dai, R.; Mateen, M.; Hassan, Z.; Zhuang, Z.; Liu, C.; Israr, M.; Cheong, W.-C.; Hu, B.; Tu, R.; et al. Cobalt Single Atom Incorporated in Ruthenium Oxide Sphere: A Robust Bifunctional Electrocatalyst for HER and OER. *Angew. Chem. Int. Ed.* **2022**, *61*, e202114951. [[CrossRef](#)] [[PubMed](#)]
10. Roger, I.; Shipman, M.A.; Symes, M.D. Earth-abundant catalysts for electrochemical and photoelectrochemical water splitting. *Nat. Rev. Chem.* **2017**, *1*, 0003. [[CrossRef](#)]
11. Lukowski, M.A.; Daniel, A.S.; English, C.R.; Meng, F.; Forticaux, A.; Hamers, R.J.; Jin, S. Highly active hydrogen evolution catalysis from metallic WS₂ nanosheets. *Energy Environ. Sci.* **2014**, *7*, 2608–2613. [[CrossRef](#)]
12. Zhang, C.; Wang, P.; Li, W.; Zhang, Z.; Zhu, J.; Pu, Z.; Zhao, Y.; Mu, S. MOF-assisted synthesis of octahedral carbon-supported PtCu nanoalloy catalysts for an efficient hydrogen evolution reaction. *J. Mater. Chem. A* **2020**, *8*, 19348–19356. [[CrossRef](#)]
13. Wang, P.; Jiang, K.; Wang, G.; Yao, J.; Huang, X. Phase and Interface Engineering of Platinum-Nickel Nanowires for Efficient Electrochemical Hydrogen Evolution. *Angew. Chem. Int. Ed.* **2016**, *55*, 12859–12863. [[CrossRef](#)]
14. Kemppainen, E.; Bodin, A.; Sebok, B.; Pedersen, T.; Seger, B.; Mei, B.; Bae, D.; Vesborg, P.C.K.; Halme, J.; Hansen, O.; et al. Scalability and feasibility of photoelectrochemical H₂ evolution: The ultimate limit of Pt nanoparticle as an HER catalyst. *Energy Environ. Sci.* **2015**, *8*, 2991–2999. [[CrossRef](#)]
15. Esposito, D.V.; Hunt, S.T.; Stottlemeyer, A.L.; Dobson, K.D.; McCandless, B.E.; Birkmire, R.W.; Chen, J.G. Low-Cost Hydrogen-Evolution Catalysts Based on Monolayer Platinum on Tungsten Monocarbide Substrates. *Angew. Chem. Int. Ed.* **2010**, *49*, 9859. [[CrossRef](#)]
16. Callejas, J.F.; McEnaney, J.M.; Read, C.G.; Crompton, J.C.; Biacchi, A.J.; Popczun, E.J.; Gordon, T.R.; Lewis, N.S.; Schaak, R.E. Electrocatalytic and Photocatalytic Hydrogen Production from Acidic and Neutral-pH Aqueous Solutions Using Iron Phosphide Nanoparticles. *ACS Nano* **2014**, *8*, 11101–11107. [[CrossRef](#)] [[PubMed](#)]
17. Callejas, J.F.; Read, C.G.; Popczun, E.J.; McEnaney, J.M.; Schaak, R.E. Nanostructured Co₂P Electrocatalyst for the Hydrogen Evolution Reaction and Direct Comparison with Morphologically Equivalent CoP. *Chem. Mater.* **2015**, *27*, 3769–3774. [[CrossRef](#)]
18. Cruz-Martinez, H.; Rojas-Chavez, H.; Matadamas-Ortiz, P.T.; Ortiz-Herrera, J.C.; Lopez-Chavez, E.; Solorza-Feria, O.; Medina, D.I. Current progress of Pt-based ORR electrocatalysts for PEMFCs: An integrated view combining theory and experiment. *Mater. Today Phys.* **2021**, *19*, 100406. [[CrossRef](#)]
19. Pu, Z.; Luo, Y.; Asiri, A.M.; Sun, X. Efficient Electrochemical Water Splitting Catalyzed by Electrodeposited Nickel Diselenide Nanoparticles Based Film. *ACS Appl. Mater. Interfaces* **2016**, *8*, 4718–4723. [[CrossRef](#)]
20. Wu, Y.; Liu, X.; Han, D.; Song, X.; Shi, L.; Song, Y.; Niu, S.; Xie, Y.; Cai, J.; Wu, S.; et al. Electron density modulation of NiCo₂S₄ nanowires by nitrogen incorporation for highly efficient hydrogen evolution catalysis. *Nat. Commun.* **2018**, *9*, 1425. [[CrossRef](#)]
21. Bae, S.-Y.; Mahmood, J.; Jeon, I.-Y.; Baek, J.-B. Recent advances in ruthenium-based electrocatalysts for the hydrogen evolution reaction. *Nanoscale Horiz.* **2020**, *5*, 43–56. [[CrossRef](#)]
22. Ye, S.; Luo, F.; Xu, T.; Zhang, P.; Shi, H.; Qin, S.; Wu, J.; He, C.; Ouyang, X.; Zhang, Q.; et al. Boosting the alkaline hydrogen evolution of Ru nanoclusters anchored on B/N-doped graphene by accelerating water dissociation. *Nano Energy* **2020**, *68*, 104301. [[CrossRef](#)]

23. Li, Y.; Luo, Y.; Zhang, Z.; Yu, Q.; Li, C.; Zhang, Q.; Zheng, Z.; Liu, H.; Liu, B.; Dou, S. Implanting Ru nanoclusters into N-doped graphene for efficient alkaline hydrogen evolution. *Carbon* **2021**, *183*, 362–367. [[CrossRef](#)]
24. Gao, M.; Wang, Z.; Sun, S.; Jiang, D.; Wei, W.; Chen, M. Highly dispersed ultra-fine Ru nanoparticles anchored on nitrogen-doped carbon sheets for efficient hydrogen evolution reaction with a low overpotential. *J. Alloys Compd.* **2021**, *864*, 158174. [[CrossRef](#)]
25. Li, D.; Liu, Y.; Liu, Z.; Yang, J.; Hu, C.; Feng, L. Electrochemical hydrogen evolution reaction efficiently catalyzed by ruthenium-nitrogen coupling in defect-rich ruthenium/graphitic carbon nitride nanosheets. *J. Mater. Chem. A* **2021**, *9*, 15019–15026. [[CrossRef](#)]
26. Mahmood, J.; Li, F.; Jung, S.M.; Okyay, M.S.; Ahmad, I.; Kim, S.J.; Park, N.; Jeong, H.Y.; Baek, J.B. An efficient and pH-universal ruthenium-based catalyst for the hydrogen evolution reaction. *Nat. Nanotechnol.* **2017**, *12*, 441–446. [[CrossRef](#)] [[PubMed](#)]
27. Ejeta, S.Y.; Imae, T. Cobalt Incorporated Graphitic Carbon Nitride as a Bifunctional Catalyst for Electrochemical Water-Splitting Reactions in Acidic Media. *Molecules* **2022**, *27*, 6445. [[CrossRef](#)]
28. Zhang, J.; Xu, X.; Yang, L.; Cheng, D.; Cao, D. Single-Atom Ru Doping Induced Phase Transition of MoS₂ and S Vacancy for Hydrogen Evolution Reaction. *Small Methods* **2019**, *3*, 1900653. [[CrossRef](#)]
29. Wang, L.; Cao, L.; Liu, X.; Zhang, W.; Liu, W.; Shen, X.; Wang, Y.; Yao, T. Strong Ni–S Hybridization in a Crystalline NiS Electroacatalyst for Robust Acidic Oxygen Evolution. *J. Phys. Chem. C* **2020**, *124*, 2756–2761. [[CrossRef](#)]
30. Ruqia, B.; Kanti Kabiraz, M.; Wook Hong, J.; Choi, S.-I. Catalyst activation: Surface doping effects of group VI transition metal dichalcogenides towards hydrogen evolution reaction in acidic media. *J. Energy Chem.* **2022**, *72*, 217–240. [[CrossRef](#)]
31. Zhu, J.; Hu, L.; Zhao, P.; Lee, L.Y.S.; Wong, K.-Y. Recent Advances in Electrocatalytic Hydrogen Evolution Using Nanoparticles. *Chem. Rev.* **2020**, *120*, 851–918. [[CrossRef](#)] [[PubMed](#)]
32. Zhu, J.; Li, S.; Xiao, M.; Zhao, X.; Li, G.; Bai, Z.; Li, M.; Hu, Y.; Feng, R.; Liu, W.; et al. Tensile-strained ruthenium phosphide by anion substitution for highly active and durable hydrogen evolution. *Nano Energy* **2020**, *77*, 105212. [[CrossRef](#)]
33. Zhao, Y.; Wang, X.; Cheng, G.; Luo, W. Phosphorus-Induced Activation of Ruthenium for Boosting Hydrogen Oxidation and Evolution Electrocatalysis. *ACS Catal.* **2020**, *10*, 11751–11757. [[CrossRef](#)]
34. Liu, X.; Liu, F.; Yu, J.; Xiong, G.; Zhao, L.; Sang, Y.; Zuo, S.; Zhang, J.; Liu, H.; Zhou, W. Charge Redistribution Caused by S,P Synergistically Active Ru Endows an Ultrahigh Hydrogen Evolution Activity of S-Doped RuP Embedded in N,PS-Doped Carbon. *Adv. Sci.* **2020**, *7*, 2001526. [[CrossRef](#)] [[PubMed](#)]
35. Anjum, M.A.R.; Lee, M.H.; Lee, J.S. Boron- and Nitrogen-Codoped Molybdenum Carbide Nanoparticles Imbedded in a BCN Network as a Bifunctional Electrocatalyst for Hydrogen and Oxygen Evolution Reactions. *ACS Catal.* **2018**, *8*, 8296–8305. [[CrossRef](#)]
36. Suryawanshi, M.P.; Ghorpade, U.V.; Shin, S.W.; Suryawanshi, U.P.; Jo, E.; Kim, J.H. Hierarchically Coupled Ni:FeOOH Nanosheets on 3D N-Doped Graphite Foam as Self-Supported Electrocatalysts for Efficient and Durable Water Oxidation. *ACS Catal.* **2019**, *9*, 5025–5034. [[CrossRef](#)]
37. Joo, J.; Kim, T.; Lee, J.; Choi, S.-I.; Lee, K. Morphology-Controlled Metal Sulfides and Phosphides for Electrochemical Water Splitting. *Adv. Mater.* **2019**, *31*, 1806682. [[CrossRef](#)]
38. Shi, Y.; Zhang, B. Recent advances in transition metal phosphide nanomaterials: Synthesis and applications in hydrogen evolution reaction. *Chem. Soc. Rev.* **2016**, *45*, 1529–1541. [[CrossRef](#)] [[PubMed](#)]
39. Yang, Y.; Yu, Y.; Li, J.; Chen, Q.; Du, Y.; Rao, P.; Li, R.; Jia, C.; Kang, Z.; Deng, P.; et al. Engineering ruthenium-based electrocatalysts for effective hydrogen evolution reaction. *Nano-Micro Lett.* **2021**, *13*, 160. [[CrossRef](#)]
40. Sun, X.; Gao, X.; Chen, J.; Wang, X.; Chang, H.; Li, B.; Song, D.; Li, J.; Li, H.; Wang, N. Ultrasmall Ru Nanoparticles Highly Dispersed on Sulfur-Doped Graphene for HER with High Electrocatalytic Performance. *ACS Appl. Mater. Interfaces* **2020**, *12*, 48591–48597. [[CrossRef](#)]
41. Gao, G.; Ding, Z.; Li, F.; Li, Y.-X.; Wang, X.L.; Yao, Y.-F. Well-dispersed ZIF-derived N-doped carbon nanoframes with anchored Ru nanoclusters as HER electrocatalysts. *Int. J. Hydrogen Energy* **2022**, *47*, 14836–14846. [[CrossRef](#)]
42. Schieppati, D.; Patience, N.A.; Galli, F.; Dal, P.; Seck, I.; Patience, G.S.; Fuoco, D.; Banquy, X.; Boffito, D.C. Chemical and Biological Delignification of Biomass: A Review. *Ind. Eng. Chem. Res.* **2023**, *62*, 12757–12794. [[CrossRef](#)]
43. Li, Y.; Zhou, M.; Pang, Y.; Qiu, X. Lignin-Based Microsphere: Preparation and Performance on Encapsulating the Pesticide Avermectin. *ACS Sustain. Chem. Eng.* **2017**, *5*, 3321–3328. [[CrossRef](#)]
44. Ruiz-Duenas, F.J.; Martinez, A.T. Microbial degradation of lignin: How a bulky recalcitrant polymer is efficiently recycled in nature and how we can take advantage of this. *Microb. Biotechnol.* **2009**, *2*, 164–177. [[CrossRef](#)]
45. Figueiredo, P.; Lintinen, K.; Hirvonen, J.T.; Kostianen, M.A.; Santos, H.A. Properties and chemical modifications of lignin: Towards lignin-based nanomaterials for biomedical applications. *Prog. Mater. Sci.* **2018**, *93*, 233–269. [[CrossRef](#)]
46. Liu, S.; Wei, W.; Wu, S.; Zhang, F. Preparation of hierarchical porous activated carbons from different industrial lignin for highly efficient adsorption performance. *J. Porous Mater.* **2020**, *27*, 1523–1533. [[CrossRef](#)]
47. Xi, Y.; Huang, S.; Yang, D.; Qiu, X.; Su, H.; Yi, C.; Li, Q. Hierarchical porous carbon derived from the gas-exfoliation activation of lignin for high-energy lithium-ion batteries. *Green Chem.* **2020**, *22*, 4321–4330. [[CrossRef](#)]
48. Zhou, B.; Li, J.; Liu, W.; Jiang, H.; Li, S.; Tan, L.; Dong, L.; She, L.; Wei, Z. Functional-Group Modification of Kraft Lignin for Enhanced Supercapacitors. *ChemSusChem* **2020**, *13*, 2628–2633. [[CrossRef](#)]

49. Guo, N.; Li, M.; Sun, X.; Wang, F.; Yang, R. Enzymatic hydrolysis lignin derived hierarchical porous carbon for supercapacitors in ionic liquids with high power and energy densities. *Green Chem.* **2017**, *19*, 2595–2602. [[CrossRef](#)]
50. Jin, Y.; Quan, J.; Wang, Y.; Li, Z. Ammoxidation of wheat straw alkaline lignin by hydrogen peroxide. II. Effect of ammoxidation on main functional groups of lignin. *Xianweisu Kexue Yu Jishu* **2001**, *9*, 21–26.
51. Zhang, K.; Han, P.; Gu, L.; Zhang, L.; Liu, Z.; Kong, Q.; Zhang, C.; Dong, S.; Zhang, Z.; Yao, J.; et al. Synthesis of Nitrogen-Doped MnO/Graphene Nanosheets Hybrid Material for Lithium Ion Batteries. *ACS Appl. Mater. Interfaces* **2012**, *4*, 658–664. [[CrossRef](#)] [[PubMed](#)]
52. Jin, Y.; Wang, Y.; Quan, J.; Li, Z. Ammoxidation of wheat straw alkaline lignin by hydrogen peroxide. III. Effect of transitional metal ions on ammoxidation reaction. *Xianweisu Kexue Yu Jishu* **2001**, *9*, 27–32.
53. Dai, Y.; Jiang, H.; Hu, Y.; Fu, Y.; Li, C. Controlled Synthesis of Ultrathin Hollow Mesoporous Carbon Nanospheres for Supercapacitor Applications. *Ind. Eng. Chem. Res.* **2014**, *53*, 3125–3130. [[CrossRef](#)]
54. Chattot, R.; Le Bacq, O.; Beermann, V.; Kühl, S.; Herranz, J.; Henning, S.; Kühn, L.; Asset, T.; Guétaz, L.; Renou, G.; et al. Surface distortion as a unifying concept and descriptor in oxygen reduction reaction electrocatalysis. *Nat. Mater.* **2018**, *17*, 827–833. [[CrossRef](#)]
55. Wu, Z.-S.; Ren, W.; Xu, L.; Li, F.; Cheng, H.-M. Doped Graphene Sheets As Anode Materials with Superhigh Rate and Large Capacity for Lithium Ion Batteries. *ACS Nano* **2011**, *5*, 5463–5471. [[CrossRef](#)]
56. Wang, Z.; Xiong, X.; Qie, L.; Huang, Y. High-performance lithium storage in nitrogen-enriched carbon nanofiber webs derived from polypyrrole. *Electrochim. Acta* **2013**, *106*, 320–326. [[CrossRef](#)]
57. Wang, H.; Zhang, C.; Liu, Z.; Wang, L.; Han, P.; Xu, H.; Zhang, K.; Dong, S.; Yao, J.; Cui, G. Nitrogen-doped graphene nanosheets with excellent lithium storage properties. *J. Mater. Chem.* **2011**, *21*, 5430–5434. [[CrossRef](#)]
58. Lu, Q.; Wang, A.-L.; Gong, Y.; Hao, W.; Cheng, H.; Chen, J.; Li, B.; Yang, N.; Niu, W.; Wang, J.; et al. Crystal phase-based epitaxial growth of hybrid noble metal nanostructures on 4H/fcc Au nanowires. *Nat. Chem.* **2018**, *10*, 456–461. [[CrossRef](#)]
59. Chopra, S.; Deshpande, R.; Naik, G.; Deshmukh, K.A.; Deshmukh, A.D.; Peshwe, D.R. Effect of microwave treatment exposure time on functionalization and purification of multi-walled carbon nanotubes (MWCNTs). *Appl. Phys. A Mater. Sci. Process.* **2019**, *125*, 855. [[CrossRef](#)]
60. Zhang, J.; Liu, P.; Wang, G.; Zhang, P.P.; Zhuang, X.D.; Chen, M.W.; Weidinger, I.M.; Feng, X.L. Ruthenium/nitrogen-doped carbon as an electrocatalyst for efficient hydrogen evolution in alkaline solution. *J. Mater. Chem. A* **2017**, *5*, 25314–25318. [[CrossRef](#)]
61. Su, J.; Yang, Y.; Xia, G.; Chen, J.; Jiang, P.; Chen, Q. Ruthenium-cobalt nanoalloys encapsulated in nitrogen-doped graphene as active electrocatalysts for producing hydrogen in alkaline media. *Nat. Commun.* **2017**, *8*, 14969. [[CrossRef](#)]
62. Kamil, A.M.; Mohammed, H.T.; Balakit, A.A.; Hussein, F.H.; Bahnemann, D.W.; El-Hiti, G.A. Synthesis, Characterization and Photocatalytic Activity of Carbon Nanotube/Titanium Dioxide Nanocomposites. *Arab. J. Sci. Eng.* **2018**, *43*, 199–210. [[CrossRef](#)]
63. Xu, X.; Zhang, S.; Tang, J.; Pan, L.; Eguchi, M.; Na, J.; Yamauchi, Y. Nitrogen-doped nanostructured carbons: A new material horizon for water desalination by capacitive deionization. *EnergyChem* **2020**, *2*, 100043. [[CrossRef](#)]
64. Ismagilov, Z.R.; Shalagina, A.E.; Podyacheva, O.Y.; Ischenko, A.V.; Kibis, L.S.; Boronin, A.I.; Chesalov, Y.A.; Kochubey, D.I.; Romanenko, A.I.; Anikeeva, O.B.; et al. Structure and electrical conductivity of nitrogen-doped carbon nanofibers. *Carbon* **2009**, *47*, 1922–1929. [[CrossRef](#)]
65. Xu, X.; Allah, A.E.; Wang, C.; Tan, H.; Farghali, A.A.; Khedr, M.H.; Malgras, V.; Yang, T.; Yamauchi, Y. Capacitive deionization using nitrogen-doped mesostructured carbons for highly efficient brackish water desalination. *Chem. Eng. J.* **2019**, *362*, 887–896. [[CrossRef](#)]
66. Yao, H.; Wang, X.; Li, K.; Li, C.; Zhang, C.; Zhou, J.; Cao, Z.; Wang, H.; Gu, M.; Huang, M.; et al. Strong electronic coupling between ruthenium single atoms and ultrafine nanoclusters enables economical and effective hydrogen production. *Appl. Catal. B Environ.* **2022**, *312*, 121378. [[CrossRef](#)]
67. Chen, G.; Wang, T.; Zhang, J.; Liu, P.; Sun, H.; Zhuang, X.; Chen, M.; Feng, X. Accelerated Hydrogen Evolution Kinetics on NiFe-Layered Double Hydroxide Electrocatalysts by Tailoring Water Dissociation Active Sites. *Adv. Mater.* **2018**, *30*, 1706279. [[CrossRef](#)]
68. Li, W.; Wei, Z.; Wang, B.; Liu, Y.; Song, H.; Tang, Z.; Yang, B.; Lu, S. Carbon quantum dots enhanced the activity for the hydrogen evolution reaction in ruthenium-based electrocatalysts. *Mater. Chem. Front.* **2020**, *4*, 277–284. [[CrossRef](#)]
69. Wang, J.; Wei, Z.; Mao, S.; Li, H.; Wang, Y. Highly uniform Ru nanoparticles over N-doped carbon: pH and temperature-universal hydrogen release from water reduction. *Energy Environ. Sci.* **2018**, *11*, 800–806. [[CrossRef](#)]
70. Liu, Y.; Chen, N.; Li, W.; Sun, M.; Wu, T.; Huang, B.; Yong, X.; Zhang, Q.; Gu, L.; Song, H.; et al. Engineering the synergistic effect of carbon dots-stabilized atomic and subnanometric ruthenium as highly efficient electrocatalysts for robust hydrogen evolution. *SmartMat* **2022**, *3*, 249–259. [[CrossRef](#)]
71. Bao, X.; Chen, Y.; Mao, S.; Wang, Y.; Yang, Y.; Gong, Y. Boosting the Performance Gain of Ru/C for Hydrogen Evolution Reaction Via Surface Engineering. *Energy Environ. Mater.* **2023**, *6*, e12418. [[CrossRef](#)]
72. Zhang, C.; Liu, Y.; Chang, Y.; Lu, Y.; Zhao, S.; Xu, D.; Dai, Z.; Han, M.; Bao, J. Component-Controlled Synthesis of Necklace-Like Hollow NiXRu Nanoalloys as Electrocatalysts for Hydrogen Evolution Reaction. *ACS Appl. Mater. Interfaces* **2017**, *9*, 17326–17336. [[CrossRef](#)] [[PubMed](#)]

73. McCrory, C.C.L.; Jung, S.; Peters, J.C.; Jaramillo, T.F. Benchmarking Heterogeneous Electrocatalysts for the Oxygen Evolution Reaction. *J. Am. Chem. Soc.* **2013**, *135*, 16977–16987. [[CrossRef](#)] [[PubMed](#)]
74. Yang, L.; Li, H.; Yu, Y.; Wu, Y.; Zhang, L. Assembled 3D MOF on 2D Nanosheets for Self-boosting Catalytic Synthesis of N-doped Carbon Nanotube Encapsulated Metallic Co Electrocatalysts for Overall Water Splitting. *Appl. Catal. B* **2020**, *271*, 118939. [[CrossRef](#)]

Disclaimer/Publisher's Note: The statements, opinions and data contained in all publications are solely those of the individual author(s) and contributor(s) and not of MDPI and/or the editor(s). MDPI and/or the editor(s) disclaim responsibility for any injury to people or property resulting from any ideas, methods, instructions or products referred to in the content.